Supporting Information

Intrinsically Stretchable Integrated Passive Matrix Electrochromic Display Using PEDOT:PSS Ionic Liquid Composite

Claire Preston, [†] *Yuta Dobashi,* [†] *Ngoc Tan Nguyen,* [†] *Mirza Saquib Sarwar,* [†] *Daniel Jun,*[‡] *Cédric Plesse,* [§] *Xavier Sallenave,* [§] *Frédéric Vidal,* [§] *Pierre-Henri Aubert,* [§] *John D. W. Madden*,*[†]

[†]Advanced Materials and Process Engineering Laboratory, Department of Electrical and Computer Engineering, University of British Columbia, Vancouver, British Columbia V6T 1Z4, Canada

[‡]Advanced Materials and Process Engineering Laboratory, Department of Chemistry, University of British Columbia, Vancouver, British Columbia V6T 1Z1, Canada

[§]CY Cergy Paris Université, CY Advanced Studies, LPPI, F-95000 Cergy, France

*Email: jmadden@ece.ubc.ca

S1. Term definitions

L^*, ΔL^* - Optical luminance and change in optical luminance, often used for representing contrast of reflective electrochromic devices, calculated from spectra and defined according to Supplementary S5.

L^*_{est}, ΔL^*_{est} - Estimated optical luminance and change in optical luminance, calculated from sRGB pixel video values similar to [1] as in Supplementary S5. Since these are not captured under standard or consistent lighting conditions between experiments, they are better for relative comparisons between similarly imaged samples. They could vary from the spectral L^* and ΔL^* by typically 5-10 units under well illuminated conditions.

R, ΔR - Reflectance and reflectance change, used for representing optical modulation of reflective electrochromic devices.

T, ΔT – Transmission and transmission change, used for representing optical modulation of transmissive electrochromic devices.

S2. PEDOT:PSS conductivity enhancements

Many approaches have been taken to enhance the conductivity of PEDOT:PSS. Some methods have also been shown to improve stretchability. Below we make a comprehensive comparison of major aspects of approaches for enhancing the conductivity of PEDOT:PSS, and include stretchability, where provided. The approach we adapted in this work is bolded, as are our results, included on the last row.

Table S1. Comparison of PEDOT:PSS Conductivity Enhancers

Additive	**Method**	**Achieved conductivity ($S \cdot cm^{-1}$)**	**Stretchability**	**Reference**
Ethylene glycol	Cosolvent	800-1460	N/A	[2–4]
DMSO	Cosolvent	800-930	N/A	[5]
DMSO/Zonyl	Cosolvent	900	10% (pre-strained substrate)	[6]
DMSO/PTSA	Cosolvent/acid	3500	N/A	[7]
PEO/Zonyl	Cosolvent polymer network	600-1230	80%	[8]
Sulfuric acid	Acid	3000	N/A	[9]
LiTFSI	Ionic salt	608-3300	133%	[10]
BMIM OSU*	**Ionic liquid**	**288 (bulk)-2544 (thin film)**	**176% (slow strain rate 10%/minute)**	**[10]**
EMIM TCB	Ionic liquid	2084	N/A	[11]
EMIM TCB	Ionic liquid	1280	50%	[12]
EMIM DCA	Ionic liquid	1126	N/A	[13]
Methanol	Alcohol	4600	N/A	[14]
BMIM OSU$	**Ionic liquid**	**447 (bulk)**	**30%**	**This work**

* Approach adapted for this work

$ This work

S3. Film characterization

For four-point measurements of PEDOT:PSS film resistance we used a custom setup with 4 spring-loaded gold-coated pins spaced by 2.54 mm that were clamped lightly onto the center of the 2.54 cm square samples. Current between 1-5 mA was run between the outer pins using an Autolab PGSTAT101, and voltage measured between the middle two pins. AFM or a Dektak profilometer was used to measure the thickness. We calculated conductivity using

$$\frac{1}{\sigma} = \frac{\pi}{ln(2)} t \left(\frac{V}{I}\right) f_2 \qquad (1)$$

where V and I are voltage and current, σ is conductivity, thickness $t << s$, the probe spacing, and f_2 is a correction factor corresponding to w/s=2.5/0.3 and l/w=2 or 1 depending on film geometry where w is width and l is length, obtained from a lookup table.[15]

S4. Electrochromic sample fabrication

Additional fabrication details: The process is shown in Figure S2. Glass slides were sonicated in acetone, ethanol, deionized water and then propanol. SEBS in toluene (20% wt) was cast onto glass, dried for 48 h, then annealed at 70ºC for 4 h. BMIM OSU in deionized water (5% wt) was added to PH1000 PEDOT:PSS dispersion to produce a final film of 46% wt BMIM OSU and stirred at 1600 RPM for 10 min. The SEBS substrates were treated with 30 W O_2 or air plasma for 3.5-4 minutes using a Harrick Basic Plasma Cleaner before spin-coating the PEDOT mixture at 1000 RPM for 60 s, followed by annealing at 130ºC for 10 min. A conductivity enhancing step was employed by soaking the film for 1 min in BMIM $OSU_{(aq)}$ solution (1% wt), spinning at 3000 RPM for 60 s and drying at 70ºC for 20 min as in previous work.[10] The carbon black/SIS electrodes were cut into pieces approximately 4 mm×8 mm and laid on the edges of the PEDOT film followed by thermal bonding by annealing at 150º C for 5 min and reinforced with epoxy resin to shield from the electrolyte and provide mechanical support. For the electrolyte, PVA (146-186k) was dissolved in deionized water at 95ºC for 2 h (10% wt), and H_3PO_4 (85% wt) was added to PVA (1.5:1 wt ratio), then stirred for 12 h at room temperature. For the opaque electrolyte, TiO_2 was added during the 12 h stirring (15% wt vs PVA). The PVA mixture was cast and dried for 48 h in ambient air, and 24 h under vacuum. Plasma treatment for 4 min was used to activate each half cell, after

which they were bonded and clamped for 2 h, and then epoxy was further used to reinforce the contact regions. The samples were additionally cut into dumbbell shapes to move stress to the central region. Following this, SPI silver paint was used to join copper tape to the carbon black traces for interfacing with external electrodes. Matrix fabrication steps are shown in Figure S8.

S5. L*a*b* calculations

For video, due to illumination non-standard and varying conditions between measurements, absolute $L^*a^*b^*$ contrast measurements could not be accurately quantified, but estimated values L^*_{est} could be obtained. These were best for comparing samples taken under similar viewing conditions. The linear video sRGB pixel values were converted to *XYZ* tristimulus and $L^*a^*b^*$ color spaces according to the definitions described in Equations (2) and (3).[16] A white backlight or Teflon background was used as a reference white with normalization performed by obtaining the white coordinates $X_nY_nZ_n$. As with convention, ΔL^* the luminance change was mainly used for representing contrast due to minimal change in a^* and b^* hue values, rather than E^*, the contrast including hue.

For conversion of spectrophotometer data to optical modulation represented by luminance change ΔL^*, Equations (2)-(5) below were used where *P* is the source power, *R* is the reflectance, and *k* is a normalization factor.[17,18] The reference white was taken as the full source transmission spectrum or the reflectance spectrum off of the reference RS50 white standard. The equations are:

$$\begin{bmatrix} X \\ Y \\ Z \end{bmatrix} = \begin{bmatrix} 0.4127 & 0.3586 & 0.1808 \\ 0.2132 & 0.7172 & 0.0724 \\ 0.0195 & 0.1197 & 0.9517 \end{bmatrix} \begin{bmatrix} R_{sRGB} \\ G_{sRGB} \\ B_{sRGB} \end{bmatrix} \quad (2)$$

$$\begin{aligned} L^* &= 116f(Y/Y_n) - 16 \\ a^* &= 500[f(X/X_n) - f(Y/Y_n)] \\ b^* &= 200[f(Y/Y_n) - f(Z/Z_n)] \end{aligned} \quad (3)$$

$$f(X/X_n) = (X/X_n)^{1/3} \text{ if } X/X_n > (24/116)^{1/3} \quad (4)$$

$$f(X/X_n) = (841/108)(X/X_n) + 16/116 \text{ if } X/X_n \leqslant (24/116)^{1/3}$$
$$\Delta E^* = \left[\left(\Delta L^*\right)^2 + \left(\Delta a^*\right)^2 + \left(\Delta b^*\right)^2\right]^{1/2} \quad (5)$$

$$X = k\int R\,(\lambda)P(\lambda)\overline{x}(\lambda)d\lambda$$
$$Y = k\int R\,(\lambda)P(\lambda)\overline{y}(\lambda)d\lambda$$
$$Z = k\int R\,(\lambda)P(\lambda)\overline{z}(\lambda)d\lambda$$
$$k = 100/\int P\,(\lambda)\overline{y}(\lambda)d\lambda$$

S6. Fiber optic spectrophotometer setup and calibration

A FormLabs Form3 3D printer was used to print custom SolidWorks-designed fixtures for transmission and reflectance measurements. Nuts were inserted and secured with cyanoacrylate glue to provide stable threading for securing collimating lenses and bolts to fasten the setup together. The setups are shown in Figures S13-S14. 10 W and 150 W tungsten halogen light sources for transmissive and reflective experiments respectively were found to exhibit <1% variation over 10 min and were filtered with dual layer 201 Lee CT Blue filters to increase 400-500 nm wavelength sensitivity, with example spectrum and variation shown in Figure S14c. For measurements, the cell was secured flat against fixture ports prior to each spectral capture. During step strain experiments, capture time was 1-3 ms averaging over 10 measurements for transmissive samples and 100 ms averaging over 1 measurement for reflective samples. The signals were observed to drop off below 450 nm, attributed to low spectral intensity and poorer fiber optic, optical component and sample material transmission of light in this region leading to lower sensitivity.

In Figure S14 we show the measurement comparisons between the Cary and Comet UV-Vis spectrophotometer systems for some samples measured with both, and in Table S2 we list the variations. For transmission, scattering by samples, optical misalignment (estimated up to 200 μm), beam nonuniformity, and small (3º) field of view of the collimating lenses mean any small deviations in alignment or focusing can have a large effect- such that it is expected our transmission values will vary between the instruments. We observed differences in average *T* measurements of up to 5%, but the variation in *ΔT* was <2%. For reflectance, we expect even more inter-instrument variation due to the difference in reflectance measurement modes used. The Cary measurements use standard integrating sphere diffuse reflectance (8º/d)

configuration (specular component included) using a DRA-2500 attachment, which measures the average diffuse reflectance from all angles of the sample, while the reflectance R600-UVVIS-SR probe measures reflectance only at the illumination angle (45º/45º), which could cause large differences in case of angular-dependent reflectance. Previous comparisons of these measurement setups reported up to 7% reflectance differences for diffuse reflective samples.[19–21] However, our samples only showed a difference in R and ΔR of maximum ~3%, indicating for our samples the unidirectional illumination and viewing did not greatly affect the measured reflectance.

Wavy structure in the spectra with effects of up to ±2.5% on T and R, but not in ΔT, and ΔR, were observed with correlation to spectral intensity, and were observed to change with optical and sample adjustments, indicating systematic offsets. Sources could include spectral intensity-dependent scattering from the sample, beam nonuniformity, and optical or sample misalignment. A previous report comparing integrating sphere to reflectance probes also reported a wavy structure, attributed to potentially surface scattering or interference behavior.[22]

Table S2 summarizes estimates of uncertainty and instrumental variation for our custom measurement system, overall indicating our setup may have higher accuracy in representing spectral changes rather than absolute values of T and R, consistent with previous reports for reflectance probe measurements. Overall, the transmission (T) and reflectance (R) measurements were found to be within 3% of T or R of values for unstrained sample modulation compared against a standard Cary 7000 UV-Vis spectrophotometer between 500-675 nm, and the ΔT, ΔR values within 2%.

S7. Cell cyclability

Figure 2c-d and Figures S5-S7 provide typical optical modulation cycling curves. In these examples, up to 7 cycles are needed to reach full contrast, as the average cell potential reaches a new steady state, similar to previous reports.[1,23,24] For the tested transmissive and reflective samples switching between 0 and -1.6 V (ΔV=1.6 V), 90% retention of ΔT or ΔR was observed after 60 cycles, while a reflective sample switched between -1.6 to +1.6 V (ΔV=3.2 V) showed 90% retention after 21 cycles, indicating faster degradation, possibly due to larger switching voltage.

Pseudoreference electrodes inserted into the cell can be used to probe half-cell potentials *vs.* ps-Ag/AgCl, revealing voltage division and reaction potentials. Similar to Figure 1c, contrast, current, and half-cell voltages are shown in Figure S3a-b for both the reflective 2 electrode and transmissive 3 electrode configurations, depicted in Figure S3c and d respectively, allowing us to examine where the reactions occur *vs.* ps-Ag/AgCl. In all cells, the oxidizing electrode reaches a voltage plateau, which corresponds to the maximum contrast and current. Additional voltage application doesn't cause more contrast or current, possibly reaching a charge compensation limit, potentially with the beginning of the overoxidation of PEDOT.[24] When the working electrode is driven to oxidize beyond the plateau in a 3-electrode arrangement as in Figure S3b, the counter electrode reducing experiences a sudden jump in potential (-5 V *vs.* ps-Ag/AgCl) and current in order to provide the compensating charge, appearing to cause permanent loss of electroactivity in one or both electrodes on subsequent cycles.

Although TiO_2 has been shown to stabilize electrochromic and electrochemical systems by acting to prevent ion incorporation,[25] widen the potential window, increase capacitance via double layer or Ti^{4+}/Ti^{3+} pair charge storage,[26] improve ionic conductivity, and reduce electrode-electrolyte interfacial resistance,[27,28] no consistent difference emerged in our TiO_2 samples from the voltage division measurements. Overall, the 3-electrode method is demonstrated as capable of probing potentials of each half cell in a stretchable solid electrochemical system, useful for investigating reactions at each electrode.

This structure of the cell is chosen to provide high stretchability, but some limitations are expected. The thickness of the PEDOT ion storage layer relative to the active layer has not been optimized, which may lead to incomplete bleaching or reduction, as previously reported in other electrochromic devices,[24,29] with such optimization having the potential to improve performance.

Stability is also imperative in moving towards consumer devices, both for electrochemical and mechanical cycling. For PEDOT:PSS electrochemical devices, degradation in performance has been attributed to chemical parasitic side reactions,[30,31] overoxidation above 1 V *vs.* Ag/AgCl,[32,33] and intercalating ions.[34,35] Charge imbalance, asymmetric cell switching and too-high potentials may also accelerate degradation, such that our material chemistry and operating parameters may contribute to shortened electrochemical cycle life.[36] Few

stretchable electrochromic reports have tested stretchability cycling, with degradation of performance after stretching to 50% over 30 cycles reported by [37] due to delamination.

S8. Pseudoreference electrodes

Similar to [38], pseudoreference Ag/AgCl electrodes (ps-Ag/AgCl) were prepared by immersing sanded Ag wires (0.5 mm, 99.9%, Sigma) in bleach (Clorox) for 20 min. They were stored in saturated KCl (Sigma) for at least 1 h and dried for 1 h before inserting into the sample at the plasma bonding step. To confirm stability and calibrate the potential, prior to sample insertion, we used 1 mM hydroquinone (Sigma) as a known redox couple and compared the cyclic voltammograms (10 $mV \cdot s^{-1}$) produced between using ps-Ag/AgCl and standard Ag/AgCl reference electrodes as shown in Figure S12. We used $H_3PO_{4(aq)}$ (1 M) and the solid PVA/H_3PO_4 electrolyte with a Pt wire as a working and carbon paper as a counter electrode. The redox peaks in the 1 M solution are separated by approximately 30 mV while in the solid by approximately 10 mV, confirming that as concentration of H_3PO_4 increases towards the content in the solid, the potential of ps-Ag/AgCl approaches that of the standard. This confirms the stability of the electrode in this electrolyte for the period of measurement (10 min) within this window, with minimal change in the second cycle.

S9. Electrolyte characterization

For the calculation of ionic conductivity, the equation below was used, where *A* is surface area, *R* is the real part of the impedance at high frequency, *t* is thickness.

$$\sigma = \frac{t}{AR} \tag{6}$$

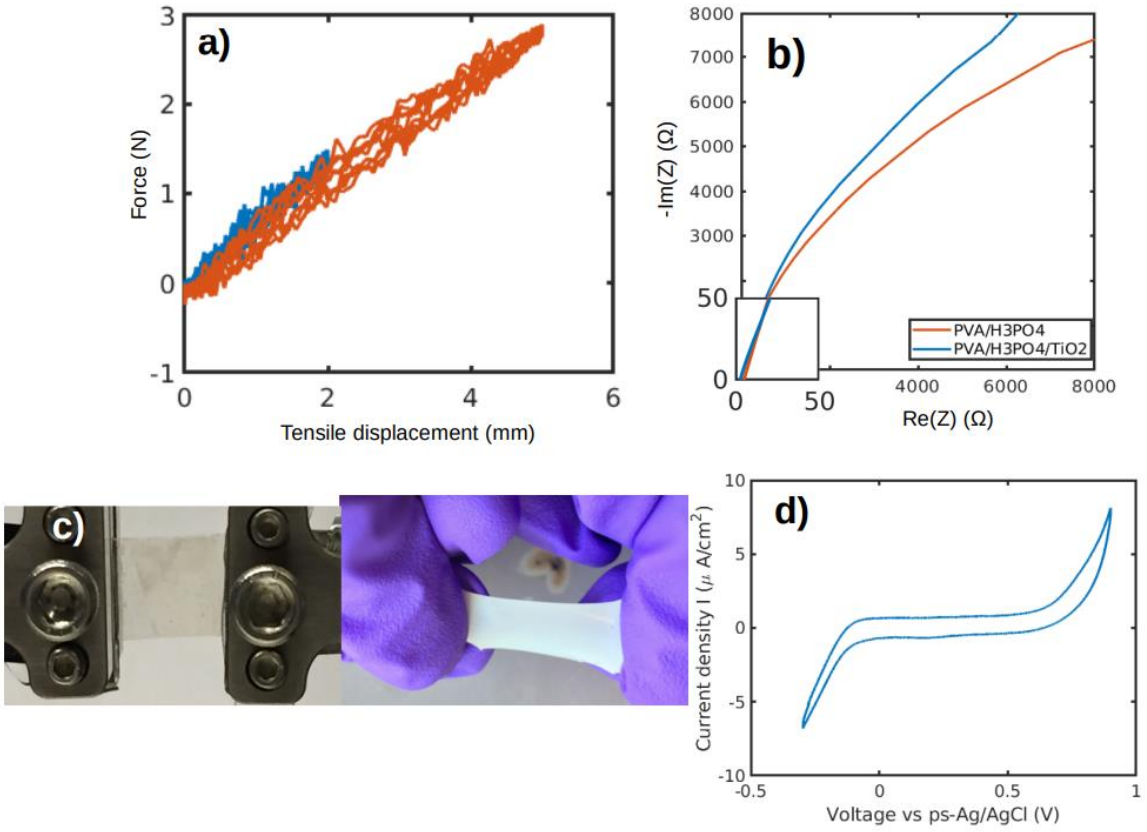

Figure S1. Electrolyte characterization. a) Force-displacement measurements of the electrolyte under sinusoidal displacement (0.1 Hz), b) impedance across electrolyte to calculate ionic conductivity (t=~200 μm), c) images of electrolytes – transmissive (left) and TiO_2-containing reflective (right), d) 3-electrode 10 $mV \cdot s^{-1}$ cyclic voltammogram of electrolyte between carbon black/SIS electrodes vs pseudoreference Ag/AgCl showing potential window.

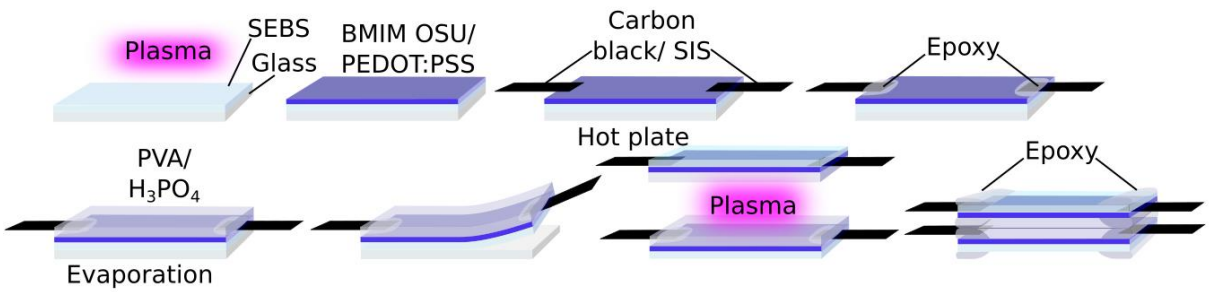

Figure S2. Fabrication steps for electrochromic single pixel. As described in the Experimental Section.

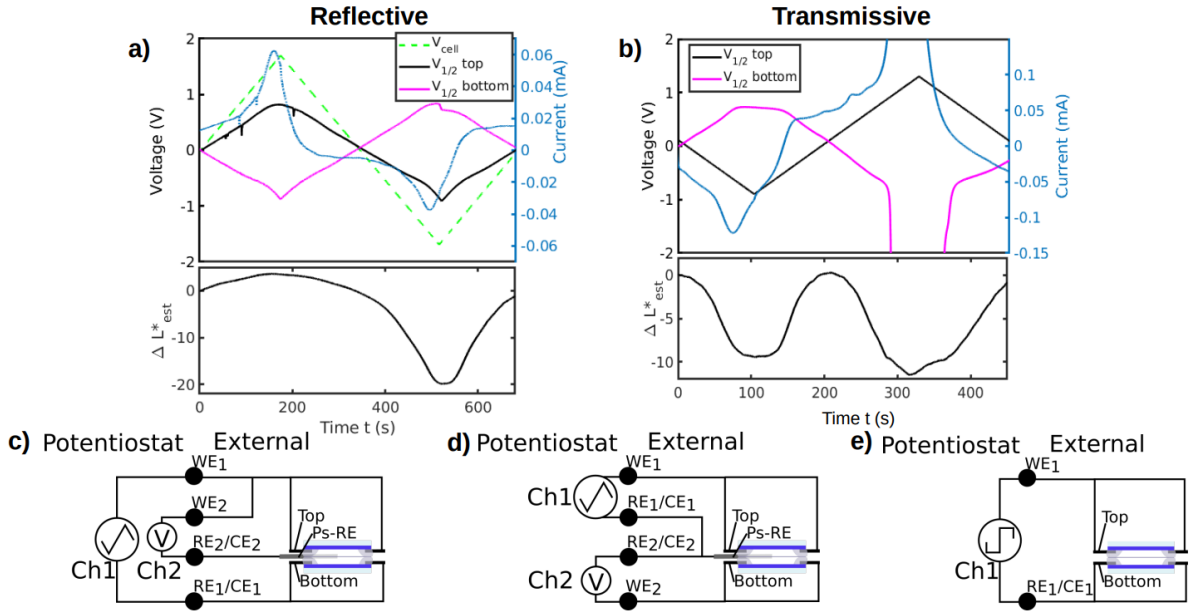

Figure S3. Three electrode characterization of electrode voltages using cyclic voltammetry. a) Cyclic voltammogram controlling working electrode (WE) (PEDOT:PSS) *vs.* counter electrode (CE) (PEDOT:PSS) and measuring between WE and ps-Ag/AgCl for reflective cell in 2 electrode configuration, b) WE (PEDOT:PSS) *vs* ps-Ag/AgCl for transmissive cell in 3 electrode configuration, c) 2 channel potentiostat configuration corresponding to Figure 1c, Figure S3a, d) 2 channel potentiostat configuration corresponding to Figure S3b, e) step potentiostat configuration corresponding to Figure 1g-l.

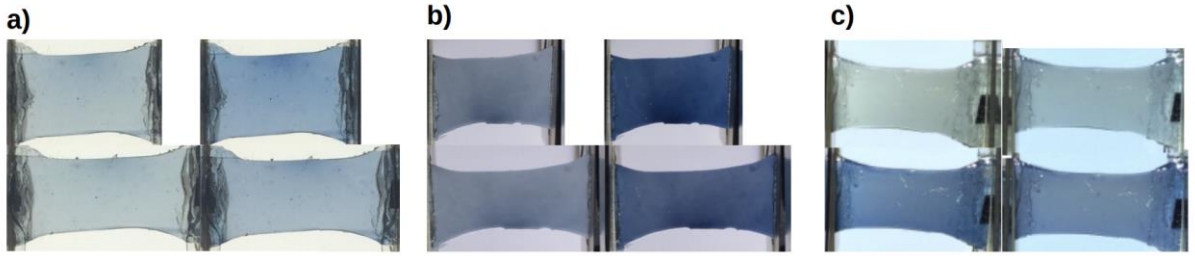

Figure S4. Original photos of electrochromic cells under 0 and 30% strain. Original photos prior to normalizing such that background reference white is equal in value to sRGB=[1 1 1] corresponding to D65 white point *XYZ*=[0.9505 1.000 0.8492], a) transmissive cell in Figure 1d, b) reflective cell in Figure 1e, c) reflective cell in Figure 2a-b

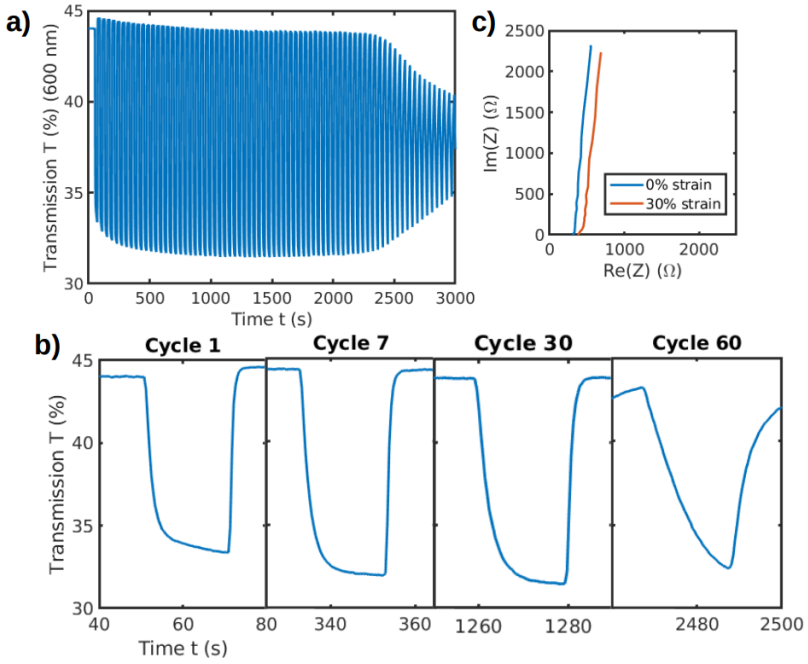

Figure S5. Transmission with electrochemical cycling of a transmissive sample under 30% strain. a) Transmission *T* (@600 nm) of transmissive sample under 30% strain over 70 electrochemical cycles (ΔV=1.6 V), b) change in optical response with cycling, c) cell impedance under strain.

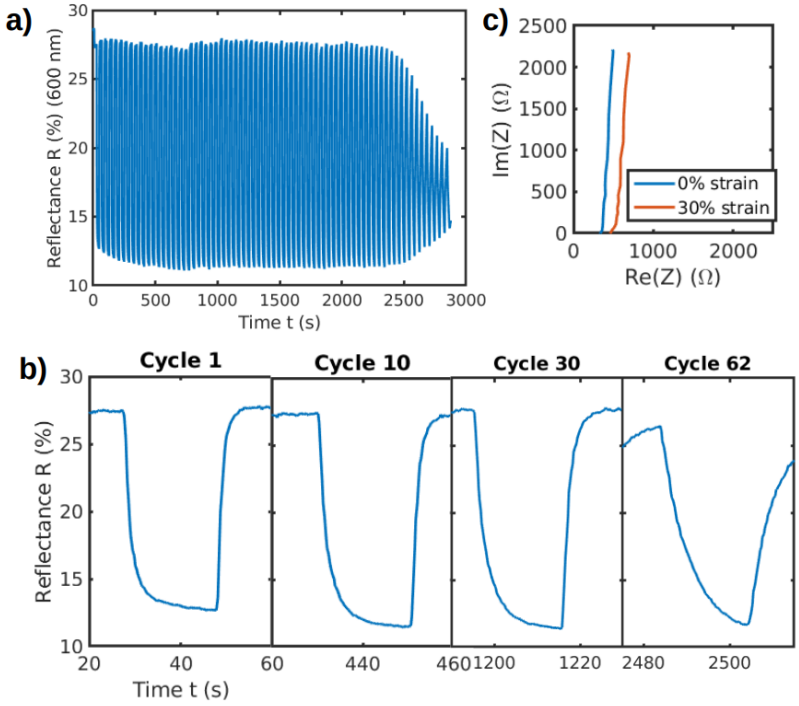

Figure S6. Reflectance with electrochemical cycling of a transmissive sample under 30% strain (ΔV=1.6 V). a) Reflectance *R* (@600 nm) of reflective sample under 30% strain over 70 electrochemical cycles (ΔV=1.6 V), b) change in optical response with cycling, c) cell impedance under strain.

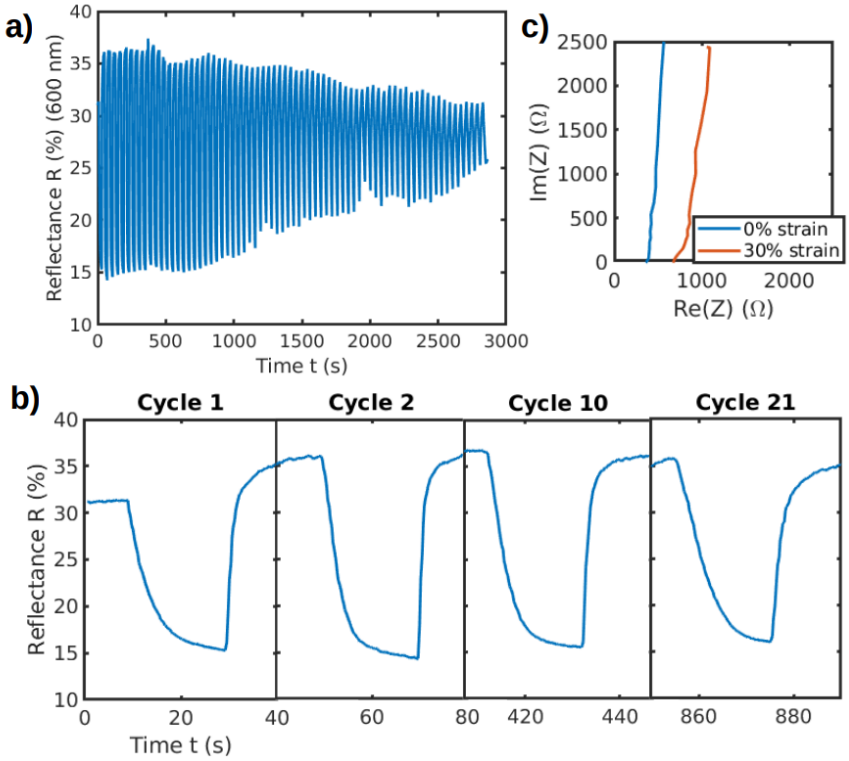

Figure S7. Reflectance with electrochemical cycling of a transmissive sample under 30% strain (ΔV=3.2 V). a) Reflectance R (@600 nm) of reflective sample under 30% strain over ~70 electrochemical cycles (ΔV=3.2 V), b) change in optical response with cycling, c) cell impedance under strain.

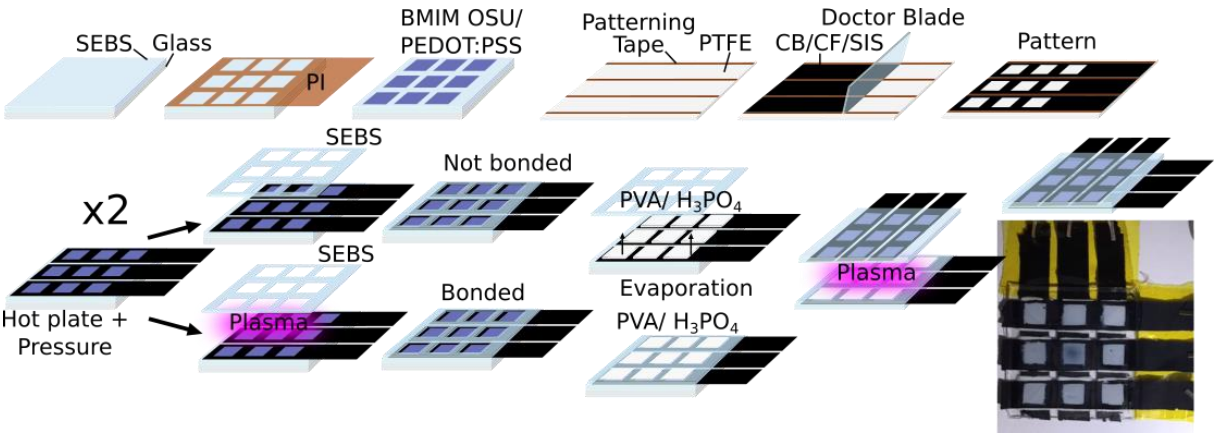

Figure S8. Fabrication steps for electrochromic matrix. Described in the main text Experimental Section. CB(carbon black)/CF(carbon nanofiber)/SIS (styrene isoprene styrene block copolymer) paste with toluene solvent is used for high conductivity electrode traces.

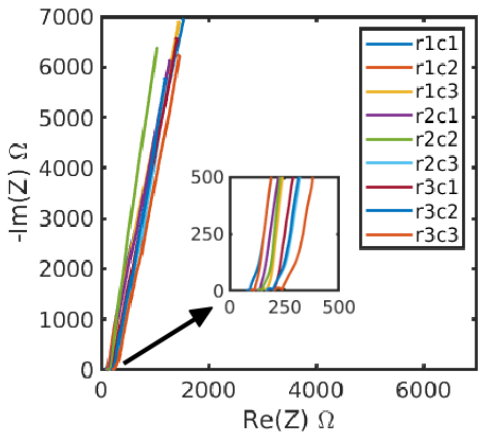

Figure S9. Electrochemical impedance spectroscopy measurements on matrix display. Electrochemical impedance spectroscopy on each row/column combination for the matrix display showing similar resistance and capacitance not greatly affected by long carbon traces or pixel fabrication variation.

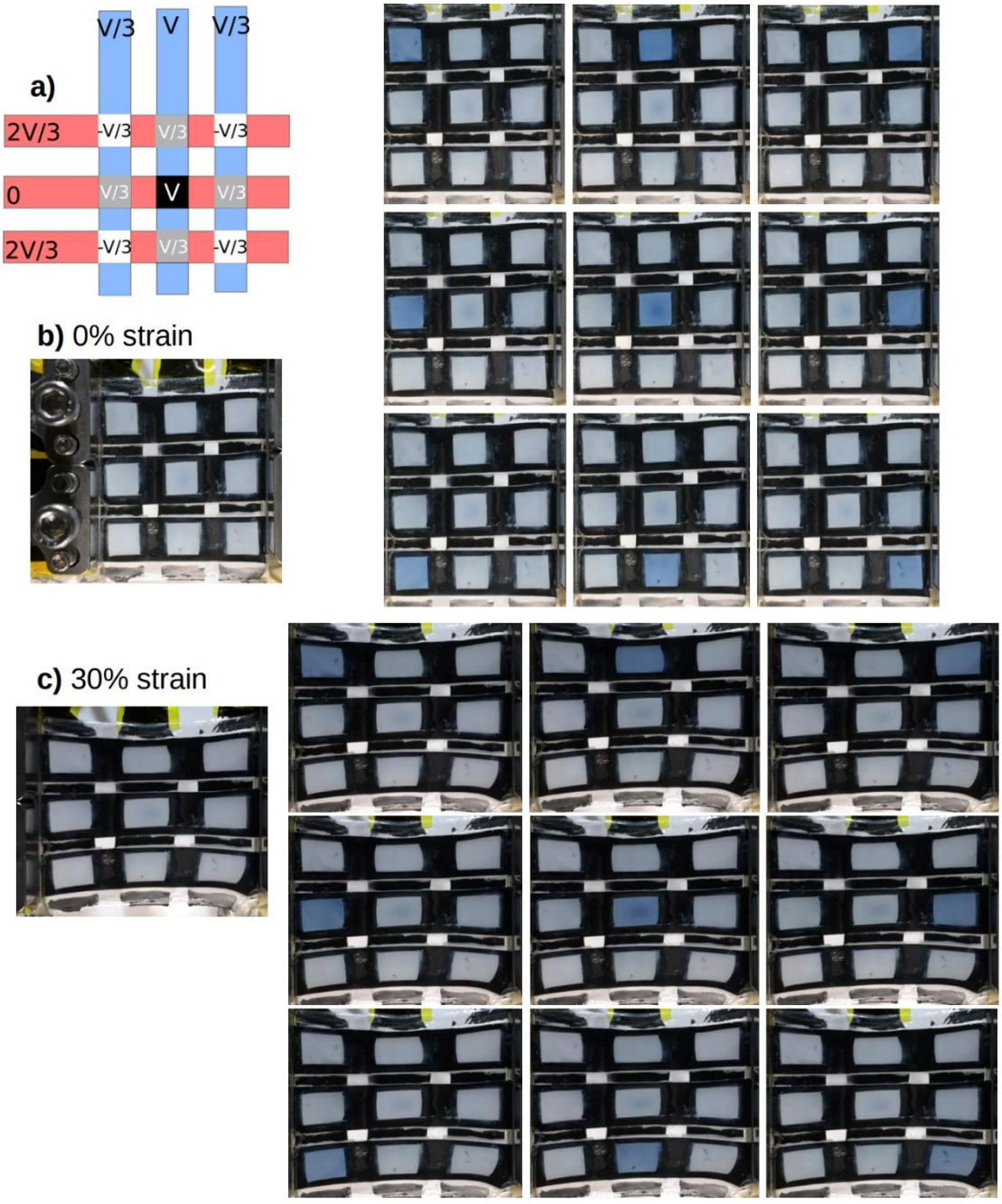

Figure S10. Single pixel addressability of matrix under 0 and 30% strain. a) *V*/3 protocol diagram demonstrating partial voltage scheme, b) switching on of sequential pixels using *V*/3 addressing protocol under 0% and c) 30% strain.

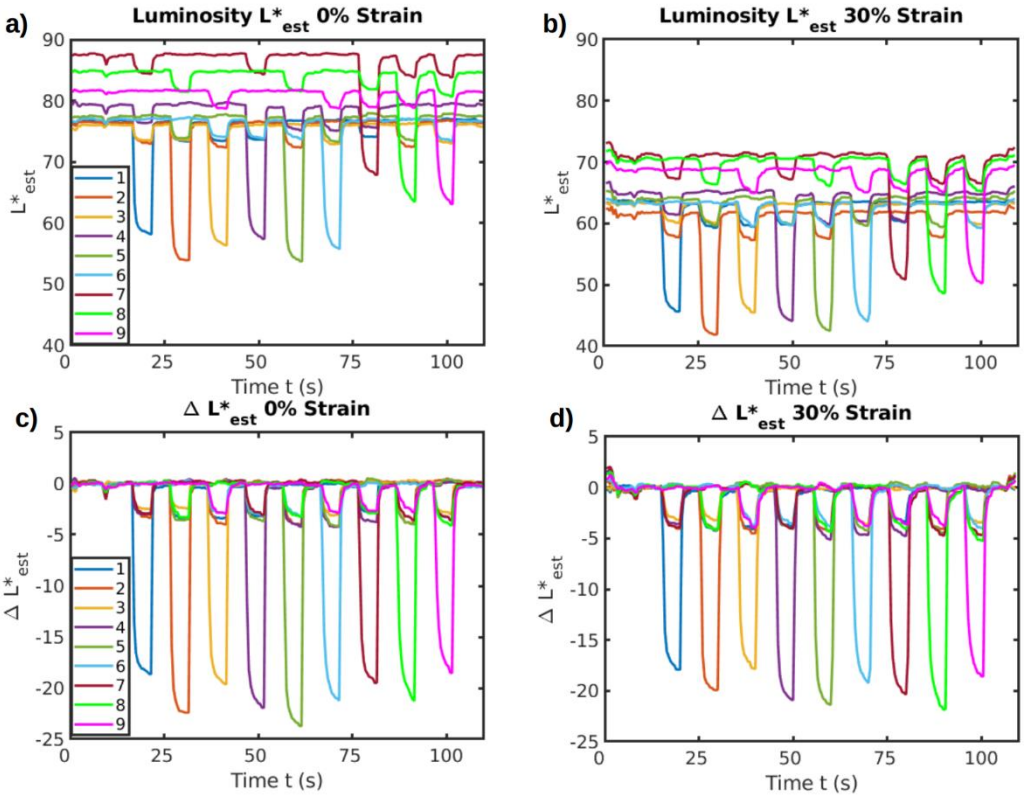

Figure S11. Luminosity measurements of pixels in matrix under 0, 30% strain. Luminosity L^*_{est} and ΔL^*_{est} of matrix under 0% and 30% strain from video for pixels 1-9, showing optical luminance change and low crosstalk for each activated pixel, a) L^*_{est} (0% strain), 5 s steps, b) L^*_{est} (30% strain), 5 s steps, c) ΔL^*_{est} (0% strain), 5 s steps, d) ΔL^*_{est} (30% strain), 5 s steps

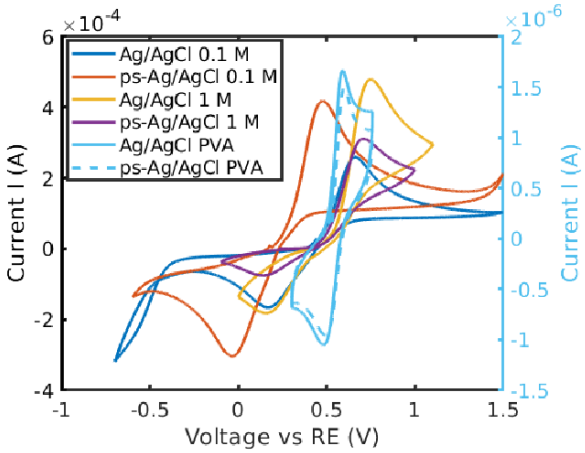

Figure S12. Cyclic voltammetry characterization of pseudoreference electrodes. Cyclic voltammetry using ps-Ag/AgCl or standard Ag/AgCl reference electrodes to compare reduction and oxidation peaks of hydroquinone in 0.1 M, 1 M H_3PO_4(aq) and solid PVA/H_3PO_4.

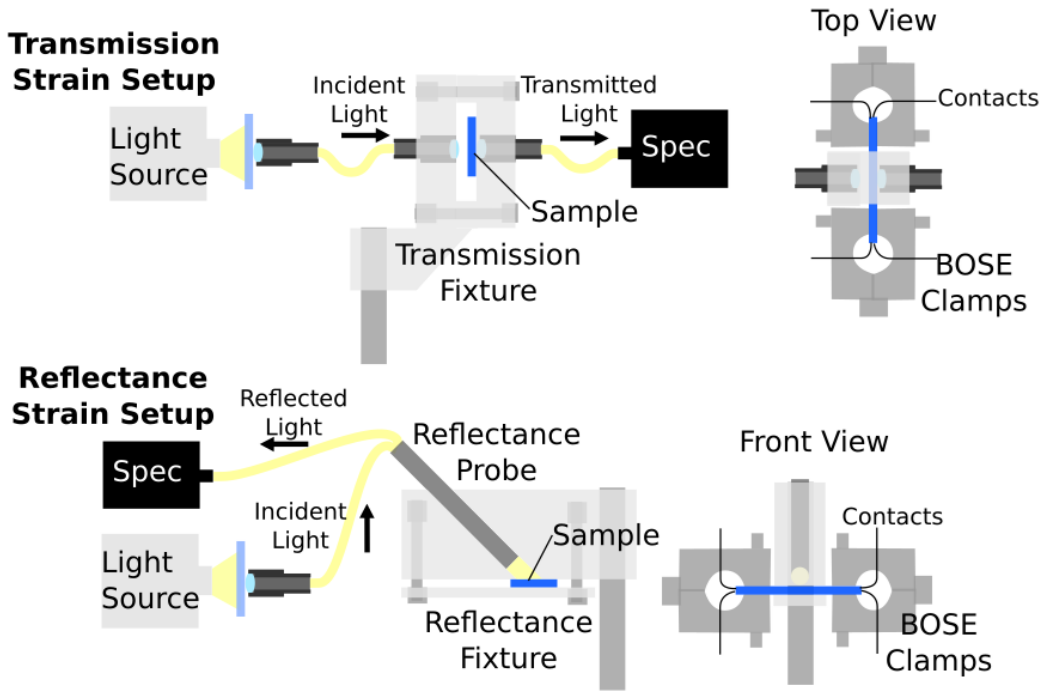

Figure S13. Transmission and reflectance setup diagrams. For measuring transmission and reflectance of samples under strain with BOSE Electroforce system and BLACK-Comet-SR spectrometer, top: transmission setup, bottom: reflectance setup.

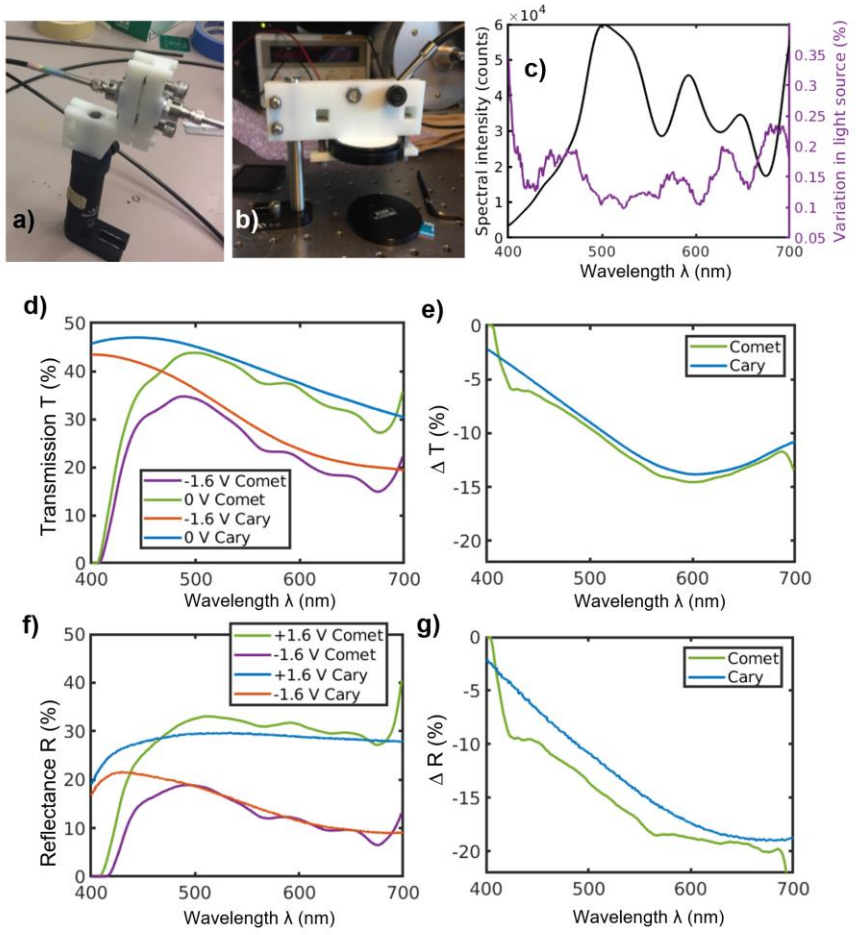

Figure S14. Transmission and reflectance fixtures and system calibration data. 3D printed a) transmission fixture, b) reflectance fixture with RS50 white standard and reflectance probe, c) filtered tungsten halogen spectrum (10 W), and comparison for calibration between Cary and Comet spectrophotometer measurements of d) T, e) ΔT for transmissive and f) R, g) ΔR for reflective samples.

Table S2. Sources of optical uncertainties and variation (500-675 nm). Comparison of transmission and reflectance measurements between measurements and compared to Cary UV-Vis 7000 for validation of StellarNet spectrometer measurements.

Average variation	Transmission	Reflectance
Random ($d\Delta T$, $d\Delta R$)		
Light source	<0.5%	<1%
Sample between cycles	2%	2%
Systematic (dT, dR)		
Instrument variation	3%	2%
Nonlinearity with source	2%	2%

Movie S1 (.mp4 format). Single transmissive and reflective pixels switching. am3c02902_si_002.mp4 demonstrates the switching of a single transmissive and reflective pixel under 0 and 30% strain.

Movie S2 (.mp4 format). Stretching and deformation of single pixel. am3c02902_si_003.mp4 shows the ability of a single pixel to continue operation under bending, folding and stretching by hand.

Movie S3 (.mp4 format). Single pixel cyclability. am3c02902_si_004.mp4 displays the operation of a single pixel at the first and 500^{th} cycles.

Movie S4 (.mp4 format). Passive matrix addressing and strain. am3c02902_si_005.mp4 demonstrates the successful addressing of single pixels in the passive matrix under 0 and 30% strain.

Movie S5 (.mp4 format). Passive matrix as a number pad. am3c02902_si_006.mp4 shows the operation of the matrix as a number pad, as a concept for wearable device development.

References

(1) Kai, H.; Suda, W.; Ogawa, Y.; Nagamine, K.; Nishizawa, M. Intrinsically Stretchable Electrochromic Display by a Composite Film of Poly(3,4-Ethylenedioxythiophene) and Polyurethane. *ACS Appl. Mater. Interfaces* **2017**, *9* (23), 19513–19518. https://doi.org/10.1021/acsami.7b03124.

(2) Rivnay, J.; Inal, S.; Collins, B. A.; Sessolo, M.; Stavrinidou, E.; Strakosas, X.; Tassone, C.; Delongchamp, D. M.; Malliaras, G. G. Structural Control of Mixed Ionic and Electronic Transport in Conducting Polymers. *Nat. Commun.* **2016**, *7*, 1–9. https://doi.org/10.1038/ncomms11287.

(3) Li, Y. Organic Optoelectronic Materials (Lecture Notes in Chemistry 91). In *Organic Optoelectronic Materials (Lecture Notes in Chemistry 91)*; Springer International Publishing: Switzerland, 2015; pp 367–382. https://doi.org/10.1007/978-3-319-16862-3.

(4) Wei, Q.; Mukaida, M.; Naitoh, Y.; Ishida, T. Morphological Change and Mobility Enhancement in PEDOT:PSS by Adding Co-Solvents. *Adv. Mater.* **2013**, *25* (20), 2831–2836. https://doi.org/10.1002/adma.201205158.

(5) Tu, S.; Tian, T.; Lena Oechsle, A.; Yin, S.; Jiang, X.; Cao, W.; Li, N.; Scheel, M. A.; Reb, L. K.; Hou, S.; Bandarenka, A. S.; Schwartzkopf, M.; Roth, S. V.; Müller-Buschbaum, P. Improvement of the Thermoelectric Properties of PEDOT:PSS Films via DMSO Addition and DMSO/Salt Post-Treatment Resolved from a Fundamental View. *Chem. Eng. J.* **2022**, *429* (June 2021), 132295. https://doi.org/10.1016/j.cej.2021.132295.

(6) Vosgueritchian, M.; Lipomi, D. J.; Bao, Z. Highly Conductive and Transparent PEDOT:PSS Films with a Fluorosurfactant for Stretchable and Flexible Transparent Electrodes. *Adv. Funct. Mater.* **2012**, *22* (2), 421–428. https://doi.org/10.1002/adfm.201101775.

(7) Mukherjee, S.; Singh, R.; Gopinathan, S.; Murugan, S.; Gawali, S.; Saha, B.; Biswas, J.; Lodha, S.; Kumar, A. Solution-Processed Poly(3,4-Ethylenedioxythiophene) Thin Films as Transparent Conductors: Effect of p-Toluenesulfonic Acid in Dimethyl Sulfoxide. *ACS Appl. Mater. Interfaces* **2014**, *6* (20), 17792–17803. https://doi.org/10.1021/am504150n.

(8) Dauzon, E.; Lin, Y.; Faber, H.; Yengel, E.; Sallenave, X.; Plesse, C.; Goubard, F.; Amassian, A.; Anthopoulos, T. D. Stretchable and Transparent Conductive PEDOT:PSS-Based Electrodes for Organic Photovoltaics and Strain Sensors

Applications. *Adv. Funct. Mater.* **2020**, *30* (28). https://doi.org/10.1002/adfm.202001251.

(9) Ouyang, J. "secondary Doping" Methods to Significantly Enhance the Conductivity of PEDOT:PSS for Its Application as Transparent Electrode of Optoelectronic Devices. *Displays* **2013**, *34* (5), 423–436. https://doi.org/10.1016/j.displa.2013.08.007.

(10) Wang, Y.; Zhu, C.; Pfattner, R.; Yan, H.; Jin, L.; Chen, S.; Molina-Lopez, F.; Lissel, F.; Liu, J.; Rabiah, N. I.; Chen, Z.; Chung, J. W.; Linder, C.; Toney, M. F.; Murmann, B.; Bao, Z. A Highly Stretchable, Transparent, and Conductive Polymer. *Sci. Adv.* **2017**, *3* (3), 1–11. https://doi.org/10.1126/sciadv.1602076.

(11) Badre, C.; Marquant, L.; Alsayed, A. M.; Hough, L. A. Highly Conductive Poly(3,4-Ethylenedioxythiophene):Poly (Styrenesulfonate) Films Using 1-Ethyl-3-Methylimidazolium Tetracyanoborate Ionic Liquid. *Adv. Funct. Mater.* **2012**, *22* (13), 2723–2727. https://doi.org/10.1002/adfm.201200225.

(12) Teo, M. Y.; Kim, N.; Kee, S.; Kim, B. S.; Kim, G.; Hong, S.; Jung, S.; Lee, K. Highly Stretchable and Highly Conductive PEDOT:PSS/Ionic Liquid Composite Transparent Electrodes for Solution-Processed Stretchable Electronics. *ACS Appl. Mater. Interfaces* **2017**, *9* (1), 819–826. https://doi.org/10.1021/acsami.6b11988.

(13) Oechsle, A. L.; Heger, J. E.; Li, N.; Yin, S.; Bernstorff, S.; Müller-Buschbaum, P. Correlation of Thermoelectric Performance, Domain Morphology and Doping Level in PEDOT:PSS Thin Films Post-Treated with Ionic Liquids. *Macromol. Rapid Commun.* **2021**, *42* (20), 1–11. https://doi.org/10.1002/marc.202100397.

(14) Worfolk, B. J.; Andrews, S. C.; Park, S.; Reinspach, J.; Liu, N.; Toney, M. F.; Mannsfeld, S. C. B.; Bao, Z. Ultrahigh Electrical Conductivity in Solution-Sheared Polymeric Transparent Films. *Proc. Natl. Acad. Sci. U. S. A.* **2015**, *112* (46), 14138–14143. https://doi.org/10.1073/pnas.1509958112.

(15) Smits, F. M. Measurement of Sheet Resistivities with the Four-Point Probe. *Bell Syst. Tech. J.* **1958**, *37*, 711–718.

(16) Anderson, M.; Motta, R.; Stokes, S. C. M. A Standard Default Color Space for the Internet - SRGB. *Color Imaging Conf.* **1996**, *8*, 238–245.

(17) Fairchild, M. D. *Color Appearance Models*, 2nd. Ed.; John Wiley and Sons, Ltd: Chichester, 2013. https://doi.org/10.1002/9781118562680.ch3.

(18) Noboru, O.; Robertson, A. R. *Colorimetry Fundamentals and Applications*; John Wiley & Sons Ltd: Chichester, 2005. https://doi.org/10.1146/annurev.matsci.30.1.117.

(19) Gargano, M.; Ludwig, N.; Pandini, D. Use of Optical Fibre in Spectrometry and

Colorimetry with Remote Probes. *J. Int. Colour Assoc.* **2012**, *8*, 36–43.

(20) Rosillo, F. G.; Alonso-García, M. C. Evaluation of Color Changes in PV Modules Using Reflectance Measurements. *Sol. Energy* **2019**, *177*, 531–537. https://doi.org/10.1016/j.solener.2018.11.039.

(21) Potůčková, M.; Červená, L.; Kupková, L.; Lhotáková, Z.; Lukeš, P.; Hanuš, J.; Novotný, J.; Albrechtová, J. Comparison of Reflectance Measurements Acquired with a Contact Probe and an Integration Sphere: Implications for the Spectral Properties of Vegetation at a Leaf Level. *Sensors* **2016**, *16* (11). https://doi.org/10.3390/s16111801.

(22) Mccarthy, W. J.; Lowry, S. *Technical Note 51695: Comparing the Performance of a Fiber Optic Probe to an Integrating Sphere*; Thermo Scientific, 2008.

(23) Chou, H.-H.; Nguyen, A.; Chortos, A.; To, J. W. F.; Lu, C.; Mei, J.; Kurosawa, T.; Bae, W.-G.; Tok, J. B.-H.; Bao, Z. A Chameleon-Inspired Stretchable Electronic Skin with Interactive Colour Changing Controlled by Tactile Sensing. *Nat. Commun.* **2015**, *6*, 8011. https://doi.org/10.1038/ncomms9011.

(24) Eric Shen, D.; Österholm, A. M.; Reynolds, J. R. Out of Sight but Not out of Mind: The Role of Counter Electrodes in Polymer-Based Solid-State Electrochromic Devices. *J. Mater. Chem. C* **2015**, *3* (37), 9715–9725. https://doi.org/10.1039/c5tc01964h.

(25) Hashimoto, S.; Matsuoka, H. Prolonged Lifetime of Electrochromism. *Surf. Interface Anal.* **1992**, *19* (1992), 464–468.

(26) Trzciński, K.; Szkoda, M.; Nowak, A. P.; Łapiński, M.; Lisowska-Oleksiak, A. Widening of the Electroactivity Potential Range by Composite Formation - Capacitive Properties of TiO2/BiVO4/PEDOT:PSS Electrodes in Contact with an Aqueous Electrolyte. *Beilstein J. Nanotechnol.* **2019**, *10*, 483–493. https://doi.org/10.3762/BJNANO.10.49.

(27) Liu, W.; Liu, N.; Sun, J.; Hsu, P. C.; Li, Y.; Lee, H. W.; Cui, Y. Ionic Conductivity Enhancement of Polymer Electrolytes with Ceramic Nanowire Fillers. *Nano Lett.* **2015**, *15* (4), 2740–2745. https://doi.org/10.1021/acs.nanolett.5b00600.

(28) Wang, W.; Alexandridis, P. Composite Polymer Electrolytes: Nanoparticles Affect Structure and Properties. *Polymers*. 2016. https://doi.org/10.3390/polym8110387.

(29) Kawahara, J.; Andersson, P.; Engquist, I.; Berggren, M. Improving the Color Switch Contrast in PEDOT : PSS-Based Electrochromic Displays. *Org. Electron.* **2012**, *13* (3), 469–474. https://doi.org/10.1016/j.orgel.2011.12.007.

(30) Kawano, K.; Pacios, R.; Poplavskyy, D.; Nelson, J.; Bradley, D. D. C.; Durrant, J. R. Degradation of Organic Solar Cells Due to Air Exposure. *Sol. Energy Mater. Sol. Cells*

2006, *90* (20), 3520–3530. https://doi.org/10.1016/j.solmat.2006.06.041.

(31) Vázquez, M.; Bobacka, J.; Ivaska, A.; Lewenstam, A. Influence of Oxygen and Carbon Dioxide on the Electrochemical Stability of Poly(3,4-Ethylenedioxythiophene) Used as Ion-to-Electron Transducer in All-Solid-State Ion-Selective Electrodes. *Sensors Actuators, B Chem.* **2002**, *82* (1), 7–13. https://doi.org/10.1016/S0925-4005(01)00983-2.

(32) Hui, Y.; Bian, C.; Wang, J.; Tong, J.; Xia, S. Comparison of Two Types of Overoxidized PEDOT Films and Their Application in Sensor Fabrication. *Sensors* **2017**, *17* (3), 2–12. https://doi.org/10.3390/s17030628.

(33) Kamensky, M. A.; Eliseeva, S. N.; Láng, G.; Ujvári, M.; Kondratiev, V. V. Electrochemical Properties of Overoxidized Poly-3,4-Ethylenedioxythiophene. *Russ. J. Electrochem.* **2018**, *54* (11), 893–901. https://doi.org/10.1134/S1023193518130219.

(34) Chen, C.-C.; Chiang, C.-Y.; Wu, T.-Y.; Sun, I.-W. Improved Electrochromic Properties of Poly(3,4-Ethylenedioxythiophene) in 1-Butyl-3-Methylimidazolium Dicyanamide. *ECS Electrochem. Lett.* **2013**, *2* (10), H43–H45. https://doi.org/10.1149/2.009310eel.

(35) Eh, A. L. S.; Tan, A. W. M.; Cheng, X.; Magdassi, S.; Lee, P. S. Recent Advances in Flexible Electrochromic Devices: Prerequisites, Challenges, and Prospects. *Energy Technol.* **2018**, *6* (1), 33–45. https://doi.org/10.1002/ente.201700705.

(36) Remmele, J.; Shen, D. E.; Mustonen, T.; Fruehauf, N. High Performance and Long-Term Stability in Ambiently Fabricated Segmented Solid-State Polymer Electrochromic Displays. *ACS Appl. Mater. Interfaces* **2015**, *7* (22), 12001–12008. https://doi.org/10.1021/acsami.5b02090.

(37) Yan, C.; Kang, W.; Wang, J.; Cui, M.; Wang, X.; Foo, C. Y.; Chee, K. J.; Lee, P. S. Stretchable and Wearable Electrochromic Devices. *ACS Nano* **2014**, No. 1, 316–322.

(38) Da Silva, E. T. S. G.; Miserere, S.; Kubota, L. T.; Merkoçi, A. Simple On-Plastic/Paper Inkjet-Printed Solid-State Ag/AgCl Pseudoreference Electrode. *Anal. Chem.* **2014**, *86* (21), 10531–10534. https://doi.org/10.1021/ac503029q.